JOURNAL OF SYNCHROTRON RADIATION

ISSN 1600-5775

Received 19 May 2022
Accepted 2 August 2022

Edited by Y. Amemiya, University of Tokyo, Japan

Keywords: topography; super-Borrmann effect.

Study of X-ray topography using the super-Borrmann effect

J. Matsui,[a] K. Takatsu[b] and Y. Tsusaka[b]*

[a]Synchrotron Radiation Research Center, Hyogo Science and Technology Association, 1-490-2 Kouto, Shingu, Tatsuno, Hyogo 679-5165, Japan, and [b]Graduate School of Science, University of Hyogo, 3-2-1 Kouto, Kamigori, Hyogo 678-1297, Japan. *Correspondence e-mail: tsusaka@sci.u-hyogo.ac.jp

X-ray topography exerting the super-Borrmann effect has been performed using synchrotron radiation to display dislocation images with a high-speed and high-resolution CMOS camera. Forward-transmitted X-rays are positively employed instead of reflected X-rays to reveal dislocations in relatively thick crystals by simultaneously exciting a pair of adjacent {111} planes owing to the super-Borrmann effect. Before the experiment, minimum values of the attenuation coefficients $A^P_{\rm min}$ for σ and π polarizations of the incident X-rays in the three-beam case are calculated. Results demonstrate that $A^P_{\rm min}$ for both polarizations are almost 20 times larger than those in the two-beam (usual Borrmann effect) case. The transmitted X-rays can be used to confirm the efficacy of taking topographs under the super-Borrmann conditions, as well as under multiple-diffraction conditions. Furthermore, super-Borrmann topographs can be considered for relatively thick crystals, where a conventional Lang X-ray topography technique is difficult to apply.

1. Introduction

The effect of anomalous transmission can be enhanced (Borrmann & Hartwig, 1965) if the Bragg condition is satisfied for the 111 and $\bar{1}11$ reflections simultaneously in the wide-angle diagram of perfect germanium (Ge) crystals with thickness t = 0.8 mm and 1.2 mm with Cu $K\alpha$ radiation. Enhanced intensity spots for the 111 and $\bar{1}11$ reflections appear at the Kossel line intersection of the T_{111} and $T_{\bar{1}11}$ traces of the reflected beams, respectively. Furthermore, enhanced intensity spots for the 111 and $\bar{1}11$ reflections appear on the R_{111} and $R_{\bar{1}11}$ traces of the transmitted (refracted in the strict sense) beams, respectively, and are symmetrical to the intersection point of the T_{111} and $T_{\bar{1}11}$ traces with respect to the respective reflecting planes. Calculation results and interpretation for the decrease in the absorption coefficient was provided (Hildebrandt, 1966, 1967) for the enhanced spots in the 111, $\bar{1}11/200$ three-beam case ($/hkl$ means χ_{g-h} when g = 111 and h = $\bar{1}11$). Later, the theoretical understanding based on detailed calculation was advanced (Feldman & Post, 1972), and was confirmed experimentally (Uebach & Hildebrandt, 1969; Hildebrandt, 1978).

Other combinations of simultaneous reflections for three-beam cases such as 111, $1\bar{1}\bar{1}/022$ (Umeno & Hildebrandt, 1975) and 220, $\bar{2}0\bar{2}/422$ (Umeno, 1972) were investigated. The Borrmann effect for four-beam and six-beam cases involving 220 reflections was found to be also enhanced (Joko & Fukuhara, 1967). Theoretical explanations were also discussed by Afanasev & Kohn (1975, 1976, 1977). This enhanced Borrmann effect is called the 'super-Borrmann' effect (Lang, 1998).

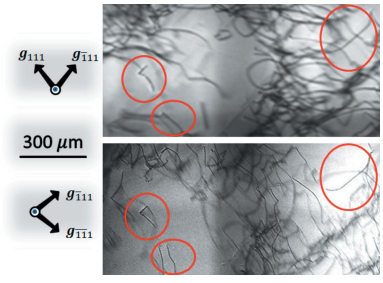

In terms of the application of the super-Borrmann effect to X-ray topography to image lattice defects in crystals, such as dislocations, as well as conventional X-ray topography, few reports have been published probably owing to a too low X-ray source intensity and large X-ray beam divergence to develop clear defect images for a wide visual field. However, since the availability of synchrotron radiation, X-ray topography can be applied for imaging lattice defects in crystals by choosing the correct X-ray wavelength. In addition, it was previously reported that topographs combined with a high-speed and high-resolution CMOS camera taken by employing forward-transmitted X-rays under multiple diffraction conditions (bright-field X-ray topographs) can reveal dislocations without noticeable image deformations (Tsusaka *et al.*, 2016, 2019).

Furthermore, as a major advantage, it is expected that the forward-transmitted X-rays riding on the super-Borrmann effect also reveal dislocations existing in relatively thick crystals by simultaneously exciting a pair of adjacent {111} planes such as (111) and $(\bar{1}11)$ where conventional Lang X-ray topography is difficult to apply. Therefore, this study deals with X-ray topography performed under three-beam multiple-diffraction conditions for thick Ge crystals using synchrotron radiation.

2. $111, \bar{1}11/200$ three-beam case

Fig. 1 shows an example of $111, \bar{1}11/200$ three-beam multiple diffraction in reciprocal space of a perfect Ge crystal. Note that the $\bar{1}11$ beam is not drawn here considering that it passes symmetrical to the 111 beam with respective to the (100) plane of symmetry in order to simplify calculation of the absorption decreases controlling the super-Borrmann effect. Figs. 1(*a*) and 1(*b*) demonstrate two cases of different energy of the incident X-rays for $E = E_1$ and $E = E_2$, respectively, which is higher than E_1. The black dashed triangle in Fig. 1 comprises the original $\mathbf{K}_o$, $\mathbf{K}_{111}$ and $\mathbf{g}_{111}$, where $\mathbf{K}_o$ is the incident X-ray wavevector, $\mathbf{K}_{111}$ is the 111-reflected X-ray wavevector and $\mathbf{g}_{111} = \mathbf{K}_{111} - \mathbf{K}_o$ is the diffraction vector of the 111 reflection lying on the same plane. Rectangles $OPQR$ and $PP'O'O$ represent projections on $(01\bar{1})$ and (100), respectively. The lengths of sides $\overline{PQ}$, $\overline{OP}$ and $\overline{PP'}$ are given as follows,

$$\overline{PQ} = \left|\overline{OQ}\right| \cos\varphi = \frac{1}{\sqrt{3}}\left|\mathbf{g}_{111}\right| = \frac{2}{\sqrt{3}}\, k \sin\theta,$$

$$\overline{OP} = \left|\overline{OQ}\right| \sin\varphi = \frac{\sqrt{2}}{\sqrt{3}}\left|\mathbf{g}_{111}\right| = \frac{\sqrt{8}}{\sqrt{3}}\, k \sin\theta,$$

$$\overline{PP'} = \overline{XL_o} = k \sin\omega,$$

where ω is an elevation angle of $\mathbf{K}_o$ (or $\mathbf{K}_{111}$) from the rectangle $OPQR$ parallel to the $(0\bar{1}1)$ entrance surface. It is clear that both $\overline{PQ}$ and $\overline{OP}$ are independent of E; however, $\overline{PP'}$ becomes larger when E increases, as observed in Figs. 1(*a*) and 1(*b*). Then, we put a unit vector of $\mathbf{K}_o$ as $\mathbf{s}_o$ and unit vectors of the polarization components of $\mathbf{K}_o$ as $\boldsymbol{\sigma}_o$ and $\boldsymbol{\pi}_o$, for horizontal and vertical polarizations, respectively. $\boldsymbol{\sigma}_o$ lies in the $(01\bar{1})$ base plane and is perpendicular to $\mathbf{s}_o$. Therefore, $\boldsymbol{\pi}_o$ is also perpendicular to $\mathbf{s}_o$ and $\boldsymbol{\sigma}_o$.

Next, we put $\mathbf{K}^s_{111[0]}$, $\mathbf{K}^\sigma_{111[0]}$ and $\mathbf{K}^\pi_{111[0]}$ in Fig. 1 as components of $\mathbf{K}_{111}$ in the $\mathbf{s}_o$, $\boldsymbol{\sigma}_o$ and $\boldsymbol{\pi}_o$ directions, respectively. The magnitudes of these vectors were calculated as $k\cos 2\theta$, $(2/\sqrt{3})\, k \sin\theta$ and $2k\sin\theta[(2/3) - \sin^2\theta]^{1/2}$, respectively. The lengths of sides $\overline{OX}$ and $\overline{XP}$ were found to have the following values,

$$\overline{OX} = \overline{QX} = \overline{QL_o}\cos\omega = k\cos\omega = \frac{\sqrt{3}}{\sqrt{8}}(2k\sin\theta) = \frac{\sqrt{3}}{\sqrt{2}}\, k\sin\theta,$$

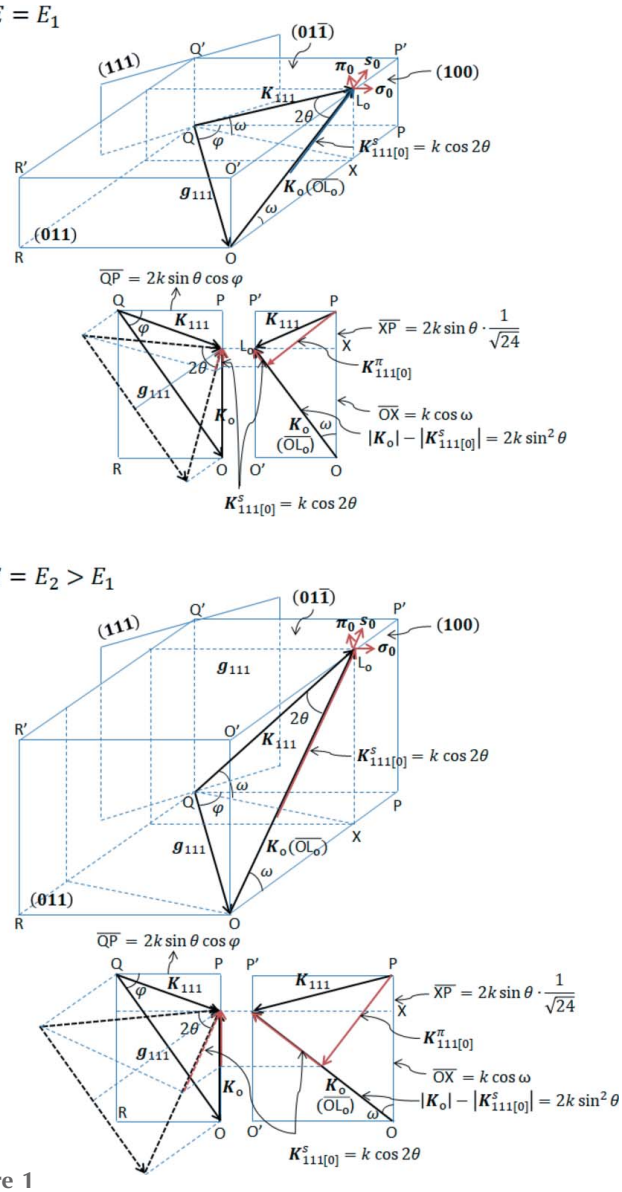

Figure 1
Schematic of $111, \bar{1}11/200$ three-beam multiple diffraction in reciprocal space of Ge, where only the 111 reflection is represented, considering the $\bar{1}11$ beam travels in a symmetrical direction with the plane of symmetry (100) at incident X-ray energies of $E = E_1$ in (*a*) and $E = E_2$ ($> E_1$) in (*b*) with rectangles $OPQR$ and $PP'O'O$ representing projections on the $(01\bar{1})$ and (100) planes, respectively. $(01\bar{1})$: entrance surface; $\mathbf{K}_o$: incident X-ray wavevector; $\mathbf{K}_{111}$: 111-reflected X-ray wavevector; $\mathbf{g}_{111}$: diffraction vector of the 111 reflection.

$$\overline{XP} = \overline{OP} - \overline{OX} = \left(\frac{\sqrt{2}}{\sqrt{3}} - \frac{\sqrt{3}}{\sqrt{8}}\right)(2k\sin\theta)$$
$$= \frac{1}{\sqrt{24}}(2k\sin\theta) = \frac{1}{3}\overline{OX}.$$

Then, we obtained $\cos\omega = (\sqrt{3}/\sqrt{2})\sin\theta$ and $\sin\omega = [1 - (3/2)\sin^2\theta]^{1/2}$ as a result for the plane parallel to the $(0\bar{1}1)$ entrance surface.

Since $\mathbf{K}_{\bar{1}11}$ is symmetrical with $\mathbf{K}_{111}$, $|\mathbf{K}^{\sigma}_{\bar{1}11[0]}| = -|\mathbf{K}^{\sigma}_{111[0]}|$; however, the $\mathbf{s}_o$, $\boldsymbol{\pi}_o$ components of $\mathbf{K}_{\bar{1}11}$ and $\mathbf{K}_{111}$ are identical. Consequently, the refracted beam $\mathbf{K}_o$ and two reflected beams $\mathbf{K}_{111}$ and $\mathbf{K}_{\bar{1}11}$ are summarized as follows,

$$\begin{pmatrix} \mathbf{K}_o \\ \mathbf{K}_{111} \\ \mathbf{K}_{\bar{1}11} \end{pmatrix} = k \begin{pmatrix} 1 & 0 & 0 \\ \cos 2\theta & -\frac{2}{\sqrt{3}}\sin\theta & 2\sin\theta\left(\frac{2}{3} - \sin^2\theta\right)^{1/2} \\ \cos 2\theta & \frac{2}{\sqrt{3}}\sin\theta & 2\sin\theta\left(\frac{2}{3} - \sin^2\theta\right)^{1/2} \end{pmatrix} \begin{pmatrix} \mathbf{s}_o \\ \boldsymbol{\sigma}_o \\ \boldsymbol{\pi}_o \end{pmatrix}. \quad (1)$$

3. Absorption coefficients in the three-beam diffraction cases

Since the calculation process for the absorption coefficient in the three-beam case under Cu $K\alpha_1$ radiation has already been provided by Authier (2001), explanation of the calculation will be kept to a minimum. Based on the fundamental equations of X-ray dynamical theory, the projections of the electric displacements $\mathbf{D}$ in the three-beam case to the plane normal to $\mathbf{K}_o$ can be written for the three beams as follows,

$$\frac{\mathbf{K}_o^2 - k^2}{k^2}\mathbf{D}_o = \chi_o\mathbf{D}_o + \chi_{\bar{1}\bar{1}\bar{1}}\mathbf{D}_{111[o]} + \chi_{1\bar{1}\bar{1}}\mathbf{D}_{\bar{1}11[o]},$$

$$\frac{\mathbf{K}_{111}^2 - k^2}{k^2}\mathbf{D}_{111} = \chi_o\mathbf{D}_{111} + \chi_{111}\mathbf{D}_{o[111]} + \chi_{200}\mathbf{D}_{\bar{1}11[111]},$$

$$\frac{\mathbf{K}_{\bar{1}11}^2 - k^2}{k^2}\mathbf{D}_{\bar{1}11} = \chi_o\mathbf{D}_{\bar{1}11} + \chi_{\bar{1}11}\mathbf{D}_{o[\bar{1}11]} + \chi_{\bar{2}00}\mathbf{D}_{[\bar{1}11]}.$$

It is possible to rewrite the above equations by using excitation errors ξ_o, ξ_{111}, $\xi_{\bar{1}11}$,

$$\begin{matrix} 2\xi_o\mathbf{D}_o & -k\chi_{\bar{1}\bar{1}\bar{1}}\mathbf{D}_{111[o]} & -k\chi_{1\bar{1}\bar{1}}\mathbf{D}_{\bar{1}11[o]} & = 0, \\ -k\chi_{111}\mathbf{D}_{o[111]} & +2\xi_{111}\mathbf{D}_{111} & -k\chi_{200}\mathbf{D}_{\bar{1}11[111]} & = 0, \\ -k\chi_{\bar{1}11}\mathbf{D}_{o[\bar{1}11]} & -k\chi_{\bar{2}00}\mathbf{D}_{111[\bar{1}11]} & +2\xi_{\bar{1}11}\mathbf{D}_{\bar{1}11} & = 0. \end{matrix} \quad (2)$$

Since the 200 reflection and $\bar{2}00$ reflectin are forbidden ($\chi_{200} = \chi_{\bar{2}00} = 0$), the above equations are expressed as follows,

$$\begin{matrix} 2\xi_o\mathbf{D}_o & -k\chi_{\bar{1}\bar{1}\bar{1}}\mathbf{D}_{111[o]} & -k\chi_{1\bar{1}\bar{1}}\mathbf{D}_{\bar{1}11[o]} & = 0, \\ -k\chi_{111}\mathbf{D}_{o[111]} & +2\xi_{111}\mathbf{D}_{111} & +0 & = 0, \\ -k\chi_{\bar{1}11}\mathbf{D}_{o[\bar{1}11]} & +0 & +2\xi_{\bar{1}11}\mathbf{D}_{\bar{1}11} & = 0. \end{matrix} \quad (3)$$

The two relations are obtained from the second and third lines of equation (3) shown above,

$$\mathbf{D}_{111} = \frac{k\chi_{111}}{2\xi_{111}}\mathbf{D}_{o[111]} = \frac{k\chi_{111}}{2\xi_{111}}\left(\mathbf{D}_o - \frac{\mathbf{K}_{111}\cdot\mathbf{D}_o}{K_{111}^2}\mathbf{K}_{111}\right),$$

$$\mathbf{D}_{\bar{1}11} = \frac{k\chi_{\bar{1}11}}{2\xi_{\bar{1}11}}\mathbf{D}_{o[\bar{1}11]} = \frac{k\chi_{\bar{1}11}}{2\xi_{\bar{1}11}}\left(\mathbf{D}_o - \frac{\mathbf{K}_{\bar{1}11}\cdot\mathbf{D}_o}{\mathbf{K}_{\bar{1}11}^2}\mathbf{K}_{\bar{1}11}\right).$$

From $\mathbf{D}_{o[111]}$ and $\mathbf{D}_{o[\bar{1}11]}$ one can obtain $\mathbf{D}_{111[o]}$ and $\mathbf{D}_{\bar{1}11[o]}$ using a vector formula $\mathbf{A}\times(\mathbf{B}\times\mathbf{C}) = (\mathbf{A}\cdot\mathbf{C})\mathbf{B} - (\mathbf{A}\cdot\mathbf{B})\mathbf{C}$ in a similar way to that described by Authier (2001). By substituting $\mathbf{D}_{111[o]}$ and $\mathbf{D}_{\bar{1}11[o]}$ thus obtained in the first line of equation (3), we obtain a relation involving only $\mathbf{D}_o$. If we decompose $\mathbf{D}_o$ into two components, D_o^{σ}, parallel to the plane of symmetry, and D_o^{π}, perpendicular to the plane of symmetry,

$$\mathbf{D}_o = D_o^{\sigma}\boldsymbol{\sigma}_o + D_o^{\pi}\boldsymbol{\pi}_o.$$

The first line of equation (2), which is

$$\mathbf{X} = 2\xi_o\mathbf{D}_o - k\chi_{\bar{1}\bar{1}\bar{1}}\mathbf{D}_{111[o]} - k\chi_{1\bar{1}\bar{1}}\mathbf{D}_{\bar{1}11[o]} = 0,$$

can be replaced using two scalar values D_o^{σ} and D_o^{π}, given as follows,

$$\mathbf{X} = AD_o^{\sigma}\boldsymbol{\sigma}_o + B(D_o^{\sigma}\boldsymbol{\pi}_o + D_o^{\pi}\boldsymbol{\sigma}_o) + CD_o^{\pi}\boldsymbol{\pi}_o = 0, \quad (4)$$

where A, B and C are the coefficients of $D_o^{\sigma}\boldsymbol{\sigma}_o$, $D_o^{\sigma}\boldsymbol{\pi}_o + D_o^{\pi}\boldsymbol{\sigma}_o$ and $D_o^{\pi}\boldsymbol{\pi}_o$, respectively,

$$A = 8\xi_o\xi_{111}\xi_{\bar{1}11} - k^2\chi_{111}\chi_{\bar{1}\bar{1}\bar{1}}\left(1 - \frac{4}{3}\sin^2\theta\right)(2\xi_{111} + 2\xi_{\bar{1}11}),$$

$$B = k^2\chi_{111}\chi_{\bar{1}\bar{1}\bar{1}}\left[\frac{4}{\sqrt{3}}\sin^2\theta\left(\frac{2}{3} - \sin^2\theta\right)^{1/2}\right](2\xi_{111} - 2\xi_{\bar{1}11}),$$

$$C = 8\,\xi_o\xi_{111}\xi_{\bar{1}11} - k^2\chi_{111}\chi_{\bar{1}\bar{1}\bar{1}}\left[1 - 4\sin^2\theta\left(\frac{2}{3} - \sin^2\theta\right)\right] \times (2\xi_{111} + 2\xi_{\bar{1}11}).$$

Considering $\mathbf{X}$ can be separated into $\boldsymbol{\sigma}_o$ and $\boldsymbol{\pi}_o$,

$$\mathbf{X} = (AD_o^{\sigma} + BD_o^{\pi})\boldsymbol{\sigma}_o + (BD_o^{\sigma} + CD_o^{\pi})\boldsymbol{\pi}_o = 0. \quad (5)$$

Therefore, we can derive the determinant as follows,

$$\begin{pmatrix} A & B \\ B & C \end{pmatrix}\begin{pmatrix} D_o^{\sigma} \\ D_o^{\pi} \end{pmatrix} = \begin{pmatrix} 0 \\ 0 \end{pmatrix},$$

and hence, inevitably,

$$\det\begin{pmatrix} A & B \\ B & C \end{pmatrix} = AC - B^2 = 0.$$

Note that the components of $\mathbf{K}_o$, $\mathbf{K}_{111}$ and $\mathbf{K}_{\bar{1}11}$ are given by equation (1) and $\xi_{111} = \xi_{\bar{1}11}$. Therefore, we understand that B vanishes, and hence AC also vanishes.

From the above considerations, A (coefficient of $D_o^{\sigma}\boldsymbol{\sigma}_o$) and C (coefficient of $D_o^{\pi}\boldsymbol{\pi}_o$) should be null independently for $\boldsymbol{\sigma}_o$ and $\boldsymbol{\pi}_o$ polarizations, respectively. As a result, we obtain

$$\xi_o\xi_{111} = \frac{1}{2}k^2\chi_{111}\chi_{\bar{1}\bar{1}\bar{1}}\left(1 - \frac{4}{3}\sin^2\theta\right)$$

for $\boldsymbol{\sigma}_o$ polarization and

$$\xi_o\xi_{111} = \frac{1}{2}k^2\chi_{111}\chi_{\bar{1}\bar{1}\bar{1}}\left[1 - 4\sin^2\theta\left(\frac{2}{3} - \sin^2\theta\right)\right]$$

for $\boldsymbol{\pi}_o$ polarization.

Considering χ_o is minimum when $|\xi_o| = |\xi_{111}|$, the subsequent values for ξ_o can be given as

$$\xi_o = -\frac{1}{\sqrt{2}}\,k\left(\chi_{111}\chi_{\bar{1}\bar{1}\bar{1}}\right)^{1/2}\left(1 - \frac{4}{3}\sin^2\theta\right)^{1/2} \qquad (6a)$$

for $\boldsymbol{\sigma}_o$ polarization and

$$\xi_o = -\frac{1}{\sqrt{2}}\,k\left(\chi_{111}\chi_{\bar{1}\bar{1}\bar{1}}\right)^{1/2}\left[1 - 4\sin^2\theta\left(\frac{2}{3} - \sin^2\theta\right)\right]^{1/2} \qquad (6b)$$

for $\boldsymbol{\pi}_o$ polarization.

In the two-beam case,

$$\xi_o\xi_{111} = \xi_o^2 = \frac{1}{4}k^2(P\chi_{111})(P\chi_{\bar{1}\bar{1}\bar{1}}).$$

When $|\xi_o| = |\xi_{111}|$, satisfying the Bragg condition exactly,

$$\xi_o = -\frac{1}{2}\,kP\left(\chi_{111}\chi_{\bar{1}\bar{1}\bar{1}}\right)^{1/2}.$$

For a cubic crystal such as Ge, the structure factor F_{111} and Fourier component of the dielectric susceptibility χ_{111} for the 111 reflection are given as follows,

$$F_{111} = 4f_{Ge}(1 + i), \qquad \chi_{111} = -\frac{r_e\lambda^2}{\pi V_c}(F_{111\_r} + iF_{111\_i}),$$

where f_{Ge} is the atomic scattering factor of Ge, r_e is the classical electron radius, λ is the wavelength of the X-rays, and V_c is the volume of a unit cell of Ge. F_{111_r} and F_{111_i} are the real and imaginary parts of the complex number F_{111}, respectively. The magnitudes of F_{111} and χ_{111} can be derived from the corresponding atomic scattering factors as follows,

$$|F_{111}| = 4\left(1^2 + |i|^2\right)^{1/2}|f| = 4\sqrt{2}\,|f_{111\_r} + f_{111\_i}|,$$

$$|\chi_{111}| = -\frac{r_e\lambda^2}{\pi V_c}\left(4\sqrt{2}\,|f_{111\_r} + f_{111\_i}|\right).$$

Then,

$$\frac{|\chi_{111\_i}|}{|\chi_{oi}|} = \frac{4\sqrt{2}f_{111\_i}}{8f_{o\_i}} = \frac{1}{\sqrt{2}}.$$

The minimum value of the absorption coefficient in the g, $h/(g-h) = 111, \bar{1}11/200$ three-beam case is given as follows,

$$\mu_e = \mu_o\left(1 - P\,\frac{|\chi_{111\_i}|}{|\chi_{o\_i}|}\right), \qquad (7)$$

where μ_o is the normal absorption coefficient and χ_{111_i} and χ_{o_i} are imaginary parts of χ_{111} and χ_o, respectively.

The minimum attenuation coefficient is $A^P_{min} = \exp[-\mu_e(t/\gamma_o)]$, where t is the slab thickness and $\gamma_o = \mathbf{n}_{hkl}\cdot\mathbf{s}_o$ is a direction cosine of the incident X-ray wavevector $\mathbf{K}_o$ (its unit vector is $\mathbf{s}_o$) to $\mathbf{n}_{hkl}$, the normal to the X-ray entrance surface. In the $111, \bar{1}11/200$ present three-beam case, it is found from Fig. 2 that the direction cosine γ_o is expressed as

$$\gamma_o = \cos\left(\frac{\pi}{2} - \omega\right) = \sin\omega = \frac{|\overline{XL_o}|}{k} = \left(1 - \frac{3}{2}\sin^2\theta\right)^{1/2}, \qquad (8)$$

for $\mathbf{K}_o$ to $\mathbf{n}_{0\bar{1}1}$.

However, the X-ray energy in the present experimental case using synchrotron radiation was E = 10 keV and the Ge slab thickness was t = 0.05 cm with the (100) entrance surface. Because the lattice parameter of Ge is a = 0.56754 nm and the Bragg angle of the 111 reflection becomes $\theta_{111} = 7.2458^\circ$ leading to $\sin\theta_{111} = 1.23984/[2(a/\sqrt{3})E] = 0.12613$, we can derive γ_o for $\mathbf{n}_{hkl} = \mathbf{n}_{001}$ from Fig. 2 as follows,

$$\gamma_o = \cos\left(\omega - \frac{\pi}{4}\right) = \frac{1}{\sqrt{2}}(\cos\omega + \sin\omega)$$
$$= \frac{1}{\sqrt{2}}\left[\sqrt{\frac{3}{2}}\sin\theta + \left(1 - \frac{3}{2}\sin^2\theta\right)^{1/2}\right] = 0.85165,$$

which corresponds to 31.608° as an angle between $\mathbf{n}_{001}$ and $\mathbf{s}_o$. In this case, the polarization factors P for the $\boldsymbol{\sigma}_o$ and $\boldsymbol{\pi}_o$ components are introduced from equation (6) as

$$P = \sqrt{2}\left(1 - \frac{4}{3}\sin^2\theta_{111}\right)^{1/2} \qquad (9a)$$

for $\boldsymbol{\sigma}_o$ polarization and

$$P = \sqrt{2}\left[1 - 4\sin^2\theta_{111}\left(\frac{2}{3} - \sin^2\theta_{111}\right)\right]^{1/2} \qquad (9b)$$

for $\boldsymbol{\pi}_o$ polarization

This makes it possible to calculate the effective absorption coefficient μ_e and the minimum attenuation coefficient A^P_{min} in the $111, \bar{1}11/200$ three-beam case for the Ge slab having the (001) entrance surface with thickness of 0.05 cm, as demonstrated in Table 1, by retrieving the data on the attenuation length from CXRO (https://henke.lbl.gov/optical_constants/

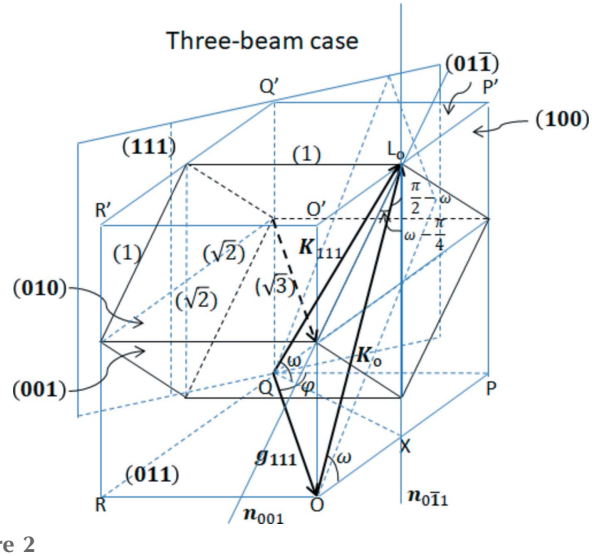

Figure 2
Schematic of the relation between $\mathbf{K}_o$, the wavevector of the incident X-rays, and $\mathbf{n}_{001}$, the (001) surface normal, or $\mathbf{n}_{0\bar{1}1}$, the $(0\bar{1}1)$ surface normal. Angles $(\pi/2) - \omega$ and $\omega - (\pi/4)$ correspond to direction cosines γ_o of $\mathbf{K}_o$ to $\mathbf{n}_{001}$ and $\mathbf{n}_{0\bar{1}1}$, respectively.

Table 1
μ_o, μ_e, A^P_{min} for $\boldsymbol{\sigma}_o$ and $\boldsymbol{\pi}_o$ polarizations in the 111, $\bar{1}11$/200 three-beam reflection case for a Ge slab (thickness: 0.05 cm; X-ray entrance surface: (100); X-ray energy: 10 keV).

Polarization	Linear absorption coefficient μ_o	Polarization component P	Effective absorption coefficient μ_e	Minimum attenuation coefficient $A^P_{min} = \exp(-\mu_e t/\gamma_o)$
$\boldsymbol{\sigma}_o$	192.213	1.380	4.638	0.672
$\boldsymbol{\pi}_o$		1.349	8.878	0.594

atten2.html). Furthermore, it was observed that A^P_{min} for both polarizations in the three-beam case are approximately 20 times the values in the two-beam case, due to which the phenomenon is called the super-Borrmann effect.

4. Topography experiment using the super-Borrmann effect for Ge crystals

To take X-ray topographs with minimized image deformation, we employed forward-transmitted (but refracted) X-rays that satisfied the Bragg conditions for the two {111} adjacent planes lying symmetrically with respect to the {100} plane of symmetry, as demonstrated in Fig. 3. An X-ray diffraction goniometer with an X-ray source of approximately 1.2 mm × 1.2 mm was used with 10 keV X-rays from the synchrotron radiation through a silicon double-crystal monochromator at the BL24XU8 beamline of SPring-8 (Tsusaka *et al.*, 2001), similar to previously reported multiple-beam diffraction topography (Tsusaka *et al.*, 2016, 2019). In order to avoid the harmonics of the incident synchrotron beam, the usual detuning treatment was carried out before carrying out the topography experiment.

Various interference patterns on diffracted and transmitted images with defect appearance were also studied using a coherent X-ray beam under multiple-diffraction conditions (Okitsu *et al.*, 2003; Okitsu, 2003). However, in the present case, topographic images were taken directly by the forward-transmitted X-ray beam instead of the diffracted X-ray beam using an X-ray imaging detector (Hondoh *et al.*, 1989). The detector comprises a 20 µm-thick $Gd_3Al_2Ga_3O_{12}$ (GAGG) scintillator, relay lens optics and a high-speed CMOS camera (Hamamatsu, C11440-22CU). This detector resolved a 1 µm line-and-space pattern.

A Ge slab of dimensions 10 mm (width) × 14 mm (height) × 0.5 mm (thickness) and the (001) surface was prepared for the super-Borrmann topography experiment. The slab was rotated in the clockwise direction around the [100] axis until bright spots corresponding to the reflections from two adjacent {111} planes, for example (111) and $(\bar{1}11)$, could be recognized on a fluorescent sheet. It is clear that this multiple (*n*-beam) diffraction from a single crystal is not considered to be so-called *umweganregung* (Reninger, 1937*a*,*b*) but simply simultaneous excitation of the plural diffractions. After confirming the double fluorescent spots by the two 111 reflections on the sheet, the images formed by the forward-transmitted beam were directly captured by the CMOS camera. As demonstrated in Fig. 3, an adjacent pair of {111} planes was selected by rotating the slab 90° clockwise around the normal to the (001) slab surface.

Figs. 4(*a*)–4(*c*) show a fluorescent spot from (*a*) the directly transmitted X-ray beam denoted as '0', (*b*) the direct beam and the 111 reflected beam, and (*c*) the direct beam, the 111 reflected beam and the $\bar{1}11$ reflected beam. It can be easily noticed that the triple fluorescent spots in Fig. 4(*c*) are much brighter than those in Fig. 4(*b*), indicating the super-Borrmann effect. The shining light on the right-hand side of Fig. 4(*c*) is due to a specular reflection by the Ge crystal surface from the 111 reflection spot on the fluorescent sheet. After the triple fluorescent spots were recognized with nearly the same brightness by sample rotation adjustment around [100] and [001], the topographic image formed by the transmitted beam was captured by the CMOS camera. During the usual Borrmann topography adjustment procedure, no clear dislocation images were recognized on the monitor.

Fig. 5 shows one of the topographs taken under the super-Borrmann conditions shown in Fig. 4(*c*) using a pair of 111 and

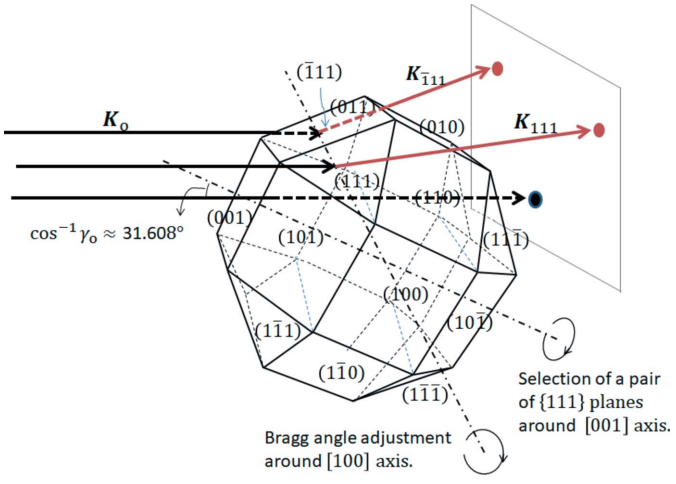

Figure 3
Incident X-rays $\mathbf{K}_o$ and reflected X-rays $\mathbf{K}_{111}$ and $\mathbf{K}_{\bar{1}11}$ simultaneously satisfying the Bragg conditions for the 111 and $\bar{1}11$ reflections, respectively, where sample rotations around [001] and [100] are performed, respectively, to select a pair of {111} planes and for Bragg condition adjustment to satisfy the individual three-beam diffraction condition.

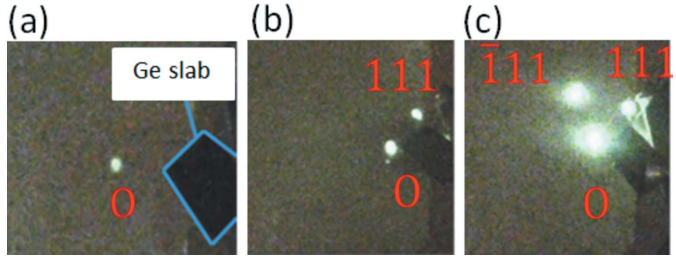

Figure 4
Reflection spots on a fluorescent sheet. (*a*) Directly transmitted X-ray beam denoted as '0', (*b*) direct beam and 111 reflected beam (suggesting the usual Borrmann case) and (*c*) direct beam and 111 and $\bar{1}11$ reflected beams (suggesting the super-Borrmann case).

$\bar{1}11$ reflections without deformation correction. Considering the X-ray source is approximately 1.2 mm × 1.2 mm in size, four shots of topographic images are pasted together to achieve a wide-area topograph. Regarding the usual Borrmann topography (two-beam case), the images of the dislocations correspond to local lower transmitted intensities (in the forward-refracted direction) or lower diffraction intensities (along the diffraction direction), since crystal imperfection can destroy the Borrmann effect. This is also true for the current super-Borrmann topography (three-beam case), since double excitation of the 111 and $\bar{1}11$ reflections only enhances the Borrmann effect, *i.e.* black contrast on the camera monitor corresponds to the local lower diffraction intensity and white contrast corresponds to the local higher intensity, a phenomenon contradictory to that on negative film.

There are four combinations of two adjacent 111 reflections, *i.e.* 111 and $\bar{1}11$ reflections (called A-type), $\bar{1}11$ and $\bar{1}\bar{1}1$ reflections (B-type), $\bar{1}\bar{1}1$ and $1\bar{1}1$ reflections (C-type), and $1\bar{1}1$ and 111 reflections (D-type). Additionally, there are two combinations of diagonal 111 reflections, *i.e.* 111 and $\bar{1}\bar{1}1$ reflections (E-type), and $\bar{1}11$ and $1\bar{1}1$ reflections (F-type). Therefore, if one observes dislocation images disappearing only in an A-type topograph, the dislocation should have a Burgers vector of $(1/2)[01\bar{1}]$, considering this vector is commonly perpendicular to both [111] and $[\bar{1}11]$. Similarly, from the invisibility rule $\mathbf{g}\cdot\mathbf{b}=0$, where $\mathbf{g}$ is the diffraction vector and $\mathbf{b}$ the dislocation Burgers vector, B-, C- and D-type topographs do not include any images of the dislocations with Burgers vectors of, respectively, (1/2)[101], (1/2)[011] and $(1/2)[\bar{1}01]$. However, the combination of diagonal 111 reflections (E- and F-type) does not develop into the super-Borrmann effect owing to the existence of χ_{220} instead of χ_{200} in equation (2). According to the partial lack of the super-Borrmann conditions, Burgers vectors of all the dislocations cannot be determined completely by only observing the A-, B-, C- and D-type topographs. Nevertheless, we can conclude that the Burgers vector of the dislocations disappearing only on the A-type topograph should belong to $(1/2)[01\bar{1}]$. For example, some parts of A- and B-type topographs are shown in Figs. 6(*a*) and 6(*b*), respectively, for the same part of the specimen. The dislocation configurations circled in red can be seen in both topographs.

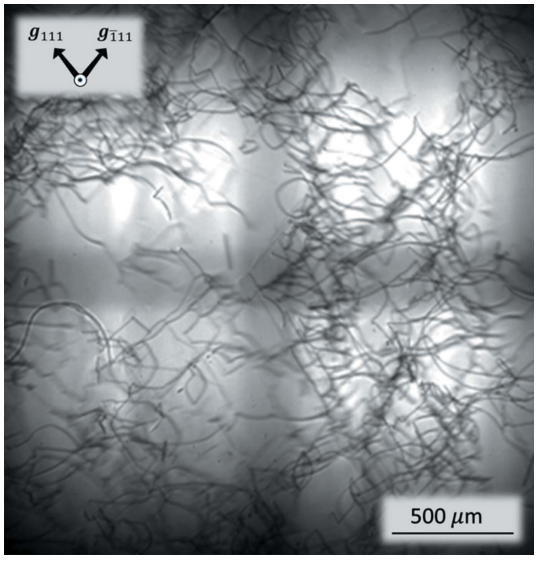

Figure 5
X-ray topograph of a germanium slab taken by simultaneous 111 and $\bar{1}11$ reflections without deformation correction. Four shots of images are pasted together to obtain a wide-area topograph.

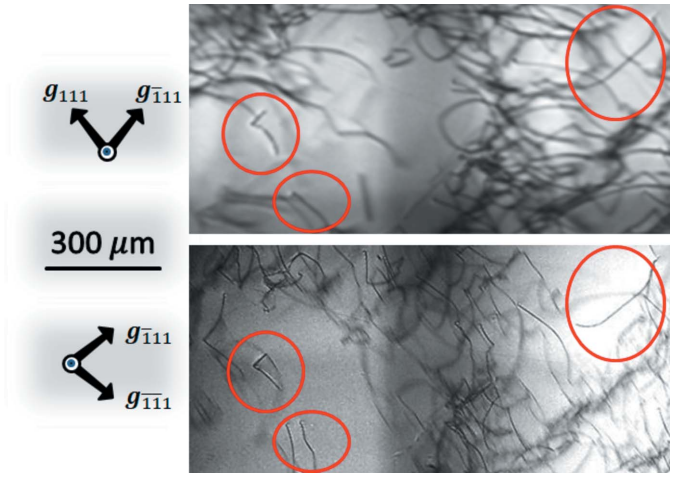

Figure 6
X-ray topographs of a germanium slab taken by (*a*) simultaneous 111 and $\bar{1}11$ reflections and (*b*) simultaneous $\bar{1}11$ and $\bar{1}\bar{1}1$ reflections with deformation correction where dislocation configurations circled in red in (*a*) and (*b*) correspond to each other.

5. Conclusions

In this study, we conducted synchrotron X-ray topography exerting the super-Borrmann effect for imaging dislocations using a CMOS camera. Forward-transmitted X-rays can reveal dislocations in relatively thick crystals by simultaneously exciting a pair of adjacent {111} planes owing to the super-Borrmann effect. Super-Borrmann topographs can be captured for relatively thick crystals, even when a conventional Lang X-ray topography technique is difficult to apply.

Prior to the experiment, the minimum attenuation coefficients $A^{\sigma}_{\rm min}$ and $A^{\pi}_{\rm min}$ for σ- and π-polarizations, respectively, of the incident X-rays in the three-beam (super-Borrmann) case were calculated. It was found that $A^{\sigma}_{\rm min}$ and $A^{\pi}_{\rm min}$ were almost 20 times larger than those in the two-beam (usual Borrmann effect) case.

Although it is possible to determine Burgers vectors for some of the dislocations based on the invisibility criteria, it is difficult to finalize the Burgers vectors of most dislocations considering that the employment of a pair of diagonal {111} planes does not produce the super-Borrmann effect.

In addition to the topographs taken by employing forward-transmitted X-rays under multiple-diffraction conditions (bright-field X-ray topographs), the forward-transmitted X-rays riding on the super-Borrmann effect also reveal dislocations existing in comparatively thick crystals by simultaneously exciting a pair of adjacent {111} planes such as (111) and $(\bar{1}11)$. Therefore, this study deals with X-ray topography

using synchrotron radiation performed under three-beam multiple diffraction conditions exerting the super-Borrmann effect for thick Ge crystals. Future research will attempt to experimentally detect dislocation behaviors around the very initial growth stage in the necking parts of dislocation-free silicon crystals.

It was clarified that forward-transmitted X-rays using synchrotron radiation can be used to confirm the efficacy for capturing topographs not only under usual multiple diffraction conditions but also under super-Borrmann conditions.

Acknowledgements

The authors would like to thank Messrs Y. Itoh and Y. Namioka for help with the X-ray topography experiments and Dr Umeno for discussions about the super-Borrmann effect. The synchrotron radiation experiments were performed at BL24XU of SPring-8 with approval from the Japan Synchrotron Radiation Research Institute (Proposal Nos. 2019B3202, 2020A3202, 2021A3202, 2021B3202).

References

Afanasev, A. M. & Kohn, V. G. (1975). *Phys. Status Solidi A*, **28**, 61–70.
Afanas'ev, A. M. & Kohn, V. G. (1976). *Acta Cryst.* A**32**, 308–310.
Afanas'ev, A. M. & Kohn, V. G. (1977). *Acta Cryst.* A**33**, 178–184.
Authier, A. (2001). *Dynamical Theory of X-ray Diffraction*, pp. 225–248. Oxford University Press.
Borrmann, G. & Hartwig, W. (1965). *Z. Krystallogr.* **121**, 401–409.
Feldman, R. & Post, B. (1972). *Phys. Status Solidi A*, **12**, 273–276.
Hildebrandt, G. (1966). *Phys. Status Solidi B*, **15**, K131–K134.
Hildebrandt, G. (1967). *Phys. Status Solidi B*, **24**, 245–261.
Hildebrandt, G. (1978). *Krist. Techn.* **13**, 1095–1104.
Hondoh, T., Goto, A., Hoshi, R., Ono, T., Anzai, H., Kawase, R., Pimienta, P. & Mae, S. (1989). *Rev. Sci. Instrum.* **60**, 2494–2497.
Joko, T. & Fukuhara, A. (1967). *J. Phys. Soc. Jpn*, **22**, 597–604.
Lang, A. R. (1998). *Cryst. Res. Technol.* **33**, 613–623.
Okitsu, K. (2003). *Acta Cryst.* A**59**, 235–244.
Okitsu, K., Imai, Y., Ueji, Y. & Yoda, Y. (2003). *Acta Cryst.* A**59**, 311–316.
Reninger, M. (1937*a*). *Z. Phys.* **106**, 141–176.
Reninger, M. (1937*b*). *Z. Kristallogr.* **97**, 107–121.
Tsusaka, Y., Mizuochi, H., Imanishi, M., Imade, M., Mori, Y. & Matsui, J. (2019). *J. Appl. Phys.* **125**, 125105.
Tsusaka, Y., Takeda, S., Takano, H., Yokoyama, K., Kagoshima, Y. & Matsui, J. (2016). *Rev. Sci. Instrum.* **87**, 023701.
Tsusaka, Y., Yokoyama, K., Takeda, S., Takai, K., Kagoshima, Y. & Matsui, J. (2001). *Nucl. Instrum. Methods Phys. Res. A*, **467–468**, 670–673.
Uebach, W. & Hildebrandt, G. (1969). *Z. Kristallogr.* **129**, 1–8.
Umeno, M. (1972). *Phys. Status Solidi A*, **11**, 501–511.
Umeno, M. & Hildebrandt, G. (1975). *Phys. Status Solidi A*, **31**, 583–594.